



A High Time-resolution Study of the Millisecond Pulsar J2241–5236 at Frequencies Below 300 MHz

D. Kaur^{1,2}, N. D. R. Bhat^{1,2}, S. E. Tremblay^{1,2}, R. M. Shannon^{3,4}, S. J. McSweeney^{1,2}, S. M. Ord⁵, A. P. Beardsley⁶, B. Crosse¹, D. Emrich¹, T. M. O. Franzen¹, L. Horsley¹, M. Johnston-Hollitt¹, D. L. Kaplan⁷, D. Kenney¹, M. F. Morales⁸, D. Pallot⁹, K. Steele¹, S. J. Tingay^{1,2}, C. M. Trott^{1,2}, M. Walker¹, R. B. Wayth^{1,2}, A. Williams¹, and C. Wu⁹

¹International Centre for Radio Astronomy Research (ICRAR), Curtin University, Bentley, WA 6102, Australia

²ARC Centre of Excellence for All-Sky Astrophysics (CAASTRO), Australia

³Centre for Astrophysics and Supercomputing, Swinburne University of Technology, P.O. Box 218, Hawthorn, VIC 3122, Australia

⁴ARC Centre of Excellence for Gravitational Wave Discovery (OzGrav), Australia

⁵CSIRO Astronomy and Space Science, P.O. Box 76, Epping, NSW 1710, Australia

⁶School of Earth and Space Exploration, Arizona State University, Tempe, AZ 85287, USA

⁷Department of Physics, University of Wisconsin–Milwaukee, Milwaukee, WI 53201, USA

⁸Department of Physics, University of Washington, Seattle, WA 98195, USA

⁹International Centre for Radio Astronomy Research, University of Western Australia, Crawley 6009, Australia

Received 2019 May 2; revised 2019 July 9; accepted 2019 July 17; published 2019 September 10

Abstract

One of the major challenges for pulsar timing array (PTA) experiments is the mitigation of the effects of the turbulent interstellar medium (ISM) from timing data. These can potentially lead to measurable delays and/or distortions in the pulse profiles and scale strongly with the inverse of the radio frequency. Low-frequency observations are therefore highly appealing for characterizing them. However, in order to achieve the necessary time resolution to resolve profile features of short-period millisecond pulsars, phase-coherent dedispersion is essential, especially at frequencies below 300 MHz. We present the lowest-frequency (80–220 MHz), coherently dedispersed detections of one of the most promising pulsars for current and future PTAs, PSR J2241–5236, using our new beamformer software for the MWA’s voltage capture system, which reconstructs the time series at a much higher time resolution of $\sim 1 \mu\text{s}$ by resynthesizing the recorded voltage data at 10 kHz/100 μs native resolutions. Our data reveal a dual-precursor type feature in the pulse profile that is either faint or absent in high-frequency observations from Parkes. The resultant high-fidelity detections have enabled dispersion measure determinations with very high precision, of the order of $(2\text{--}6) \times 10^{-6} \text{ pc cm}^{-3}$, owing to the microsecond level timing achievable for this pulsar at the MWA’s low frequencies. This underscores the usefulness of low-frequency observations for probing the ISM toward PTA pulsars and informing optimal observing strategies for PTA experiments.

Key words: instrumentation: interferometers – ISM: general – pulsars: general – pulsars: individual (PSR J2241–5236)

1. Introduction

Millisecond pulsars (MSPs) are important targets for high-precision pulsar timing array (PTA) experiments, which involve regular monitoring of pulse arrival times from a celestial distribution of pulsars to search for ultra-low-frequency (nHz) gravitational waves (e.g., van Haasteren et al. 2011; Demorest et al. 2013; Manchester et al. 2013; Janssen et al. 2015; Bailes et al. 2018). To achieve the required ~ 100 ns timing precision, it is important to ascertain various factors contributing to the timing noise budget (e.g., Cordes & Shannon 2010). PTA efforts over the past few years suggest that the interstellar medium (ISM) propagation effects on pulsar signals are one of the major contributing factors and may ultimately limit the detection sensitivity of PTAs if they are not accurately measured and corrected for in timing measurements (Cordes et al. 2016; Levin et al. 2016; Jones et al. 2017; Shannon & Cordes 2017).

The magnitudes of ISM effects scale strongly with the inverse of observing frequency. Therefore, PTAs generally observe pulsars at higher frequencies ($\sim 1\text{--}2$ GHz) to reduce the effects of the ISM (Lam et al. 2018). Two dominant effects are (1) dispersion arising from propagation through intervening ionized gas, which is quantified as the integrated electron density along the line of sight of the pulsar and is called the

dispersion measure (DM); and (2) pulse broadening arising from multipath propagation in the turbulent ISM. The dispersion delay scales as ν^{-2} , and pulse broadening time as $\sim \nu^{-4}$ (e.g., Bhat et al. 2004), where ν is the observing frequency. Low-frequency observations of pulsars can therefore allow a robust characterization of ISM effects, unlike those at higher frequencies where their impact on timing measurements are not easily discernible. Low-frequency observations can also be used to investigate the recently proposed effects such as chromatic (frequency-dependent) DM, arising due to different path lengths traversed, or volumes sampled, at different frequencies, again owing to multipath propagation (Cordes et al. 2016). This may also have important implications for timing-array applications, as that would imply that correcting for ISM effects using low-frequency data is not straightforward. Thus, detailed observational investigations over a wide range of frequencies will be very instructive.

Developments in low-frequency radio instrumentation and advances in computing over the past decade have revitalized pulsar astronomy at low frequencies. Instruments such as the Murchison Widefield Array (MWA; Tingay et al. 2013), the Low Frequency Array (LOFAR; van Haarlem et al. 2013), and the Long Wavelength Array (LWA; Taylor et al. 2012) have been built and are operational, and they are opening up new opportunities for observing pulsars at frequencies below

300 MHz. The MWA is also a low-frequency (80–300 MHz) precursor to the Square Kilometer Array (SKA). The MWA has been recently upgraded, with a doubling of the number of tiles and maximum baseline, i.e., a 256-tile array extending out to ~ 6 km (Wayth et al. 2018). With its voltage capture system (VCS; Tremblay et al. 2015), which records data at 10 kHz/100 μ s resolutions, the MWA has been producing a wide variety of pulsar science (e.g., McSweeney et al. 2017; Meyers et al. 2017; Xue et al. 2017), including characterization of the ISM toward important southern-sky PTA targets (e.g., Bhat et al. 2014, 2016, 2018).

For MSPs with short rotation periods ($P \lesssim 5$ ms; where P is the period) and narrow pulse profiles, the 10 kHz channelization of VCS limits their detection, especially at the lower frequencies of the MWA. For example, a pulsar with a DM of 10 pc cm $^{-3}$ will be smeared to 1.62 ms at 80 MHz. Fundamentally, this hampers the ability to resolve fine temporal features in the pulse profiles of MSPs. Thus, we require the ability for higher time resolution and phase-coherent dedispersion to remove temporal smearing at the low frequencies of the MWA.

In this paper, we present early science results from our new and improved beamformer software, which allows resynthesis of 1.28 MHz/0.78 μ s voltage samples from 10 kHz/100 μ s native resolutions of the VCS, by performing an inversion of the polyphase filterbank (PFB) operation that was applied prior to VCS recording. This is demonstrated using our observations of PSR J2241–5236, an important PTA target. The pulsar was discovered in targeted searches toward unassociated *Fermi*-LAT candidates, and has a period of 2.18 ms and a DM of 11.41 pc cm $^{-3}$ (Keith et al. 2011). The new beamformer has enabled pulsar detections down to ~ 80 MHz, thereby allowing us to study the ISM and spectral properties of the pulsar. In Section 2 we describe the details of our observations. In Sections 3 and 4 we summarize data processing and analysis, and in Section 5 we present our results. Our conclusions are summarized in Section 6.

2. Observations

Observations were made at three epochs, each separated by nearly ~ 1 yr, with the MWA-VCS, which records 24 coarse channels, each of which has been finely channelized to 10 kHz using a 12-tap PFB. It records both polarizations from a maximum of 128 tiles, and has an aggregate data rate of ~ 28 TB hr $^{-1}$. The 30.72 MHz observing bandwidth currently feasible with the MWA can flexibly be recorded in either a contiguous band or can be split into 24×1.28 MHz coarse channels, which can be placed anywhere across the nominal operating frequency range (80–300 MHz). This distributed channel mode is particularly suitable for exploring frequency-dependent effects such as pulse profile evolution, scintillation and scattering (Bhat et al. 2018; Kirsten et al. 2019). The VCS data are transported to the Pawsey supercomputing facility, where all further processing, including calibration and beamforming, are carried out. Further details of the observations are summarized in Table 1.

3. Data Processing

The VCS data can be processed to form a coherent beam by applying suitable phase rotations to each voltage stream and then summing them to generate a phased-array signal (Ord et al. 2019). It involves accounting for the polarimetric

Table 1
Observational Details of PSR J2241–5236

MJD	Frequency Range (MHz)	Channel Setup	Observing Duration (s)	N_{tile} ^a
57288	170–200	1×30.72	4800	114
57707	80–220	12×2.56^b	1800	126
57979	80–220	12×2.56^b	3600	121

Notes.

^a Number of tiles used while producing calibration solutions.

^b Two consecutive 1.28 MHz channels joined together.

response for each tile and frequency channel by applying appropriate cable and geometric delays and complex gains (i.e., amplitudes and phases). Data are then calibrated using standard calibrators (e.g., Hydra A and 3C444), recorded in pointed observations prior to pulsar observations. The calibration solutions are generated for each tile and frequency channel using the Real Time System (Mitchell et al. 2008), and tiles that produced poor calibration solutions are flagged. The full processing pipeline is implemented on the Galaxy cluster at the Pawsey Supercomputing Centre. These data are then processed using the standard pulsar data analysis packages DSPSR (van Straten & Bailes 2011) and PSRCHIVE (Hotan et al. 2004; van Straten et al. 2012) to generate multichannel pulse profiles for further analysis.

3.1. Reconstructing the High-time Resolution Time Series

High-quality MSP detections require coherent dedispersion, in which the received voltage signal is deconvolved using the transfer function of the ISM (Hankins & Rickett 1975). While this technique has been routinely implemented in pulsar instrumentation around the world (e.g., van Straten & Bailes 2011), it was not possible earlier with the MWA due to our fine 10 kHz channelization and the filterbank format of beamformed data (written in full-Stokes PSRFITS). With the new beamformer software, which reconstructs the data at a much higher time resolution by resynthesizing the coarse-channel voltage samples (by effectively inverting the fine PFB operation that produced the fine channels), it has become possible to generate data that are amenable for coherent dedispersion.

The MWA fine channelization is implemented via a PFB with a 12-tap Kaiser window function, which is one of a class of window functions that allows theoretically perfect inversion of the PFB channelization process (Crochiere 1983; Oppenheim et al. 1999).¹⁰ The synthesis filterbank is achieved by first up-sampling the output of each 10 kHz fine channel to the initial time resolution (a factor of 128) and then passing them through a synthesis filter, which we choose to be the same filter used in the forward PFB stage, with an appropriately chosen phase ramp applied to each fine channel. Then each channel is low-pass filtered to remove the 127 images of the spectrum created by the up-sampling. The resynthesized coarse channels have a time resolution of ~ 0.78 μ s and can be coherently dedispersed to produce high-quality detections of MSPs at the MWA’s frequencies. Further details of this are described in an upcoming publication (S. J. McSweeney et al. 2019, in preparation).

¹⁰ In practice, integer quantization in the analysis and/or synthesis process means the reconstruction will not be perfect.

4. Analysis

4.1. DM Determination

Figure 1 presents MWA detections of PSR J2241–5236 across the 80–220 MHz range. As is evident from the figure, the pulsar is visibly bright across the ~ 100 –200 MHz frequency range. Using the best detection (signal-to-noise ratio; $S/N \sim 70$), we created an analytic template, which is a noise-free profile model, composed of von Mises functions, generated using the PAAS utility of PSRCHIVE. The analytic template is then cross-correlated with the observed profiles to obtain the times of arrival (ToAs) using the PSRCHIVE package. The ToAs are then analyzed using the pulsar timing package TEMPO2 (Hobbs et al. 2006) to determine the DM. We adopted the latest available timing solution of the pulsar and only fit for DM in this analysis. As our observing system is configured as 24 individual frequency sub-bands, we derived the DM using a set of 24 ToAs for every single observation.

As seen in Figure 1, the pulse width is relatively unchanged throughout the observed frequency range,¹¹ and therefore for the purpose of the DM analysis, we assume that there is no significant pulse profile evolution within our observing band. Ideally, the profile evolution needs to be considered (see Pennucci 2019); however, our data quality is not adequate for a detailed analysis. The data are subsequently reprocessed using the refined DM to obtain better quality pulse profiles. The related analysis is illustrated in Figure 2, which shows pulsar signal across 80–220 MHz, with 12×2.56 MHz channels joined together. This detection is from MJD 57979 and corresponds to the brightest among all our observations. These profiles at 80–220 MHz are then averaged in frequency to generate a standard profile centered at 150 MHz, as shown in Figure 3, which is then used as a final template for all observations to obtain the ToAs and DM measurements.

4.2. Flux Density Calibration

The flux density calibration for our data is carried out using the approach described by Meyers et al. (2017). This involves estimating the system gain (G) by simulating the tied-array beam pattern and integrating the response across the visible sky for the phased-array configuration used for observing. The tied-array beam pattern is then combined with the Global Sky Model of de Oliveira-Costa et al. (2008) to calculate the antenna temperature (T_{ant}). Assuming a radiation efficiency (η) of unity, the system temperature (T_{sys}) is then $T_{\text{sys}} = T_{\text{ant}} + T_{\text{rec}}$, where T_{rec} is the measured receiver temperature. This process is conducted separately for each sub-band, as all of these quantities are strongly frequency dependent. While doing this, we also account for a “coherency factor” (see Meyers et al. 2017), for any loss in sensitivity in the coherent beamforming process. This information is then used to estimate the flux density for all the observed frequency bands using the radiometer equation (Lorimer & Kramer 2004) and also by factoring in the duty cycle of the pulsar, which is equivalent pulse width (W) divided by the pulse period (W/P), where W is measured as integrated flux over the “on” pulse divided by the peak amplitude of the pulse.

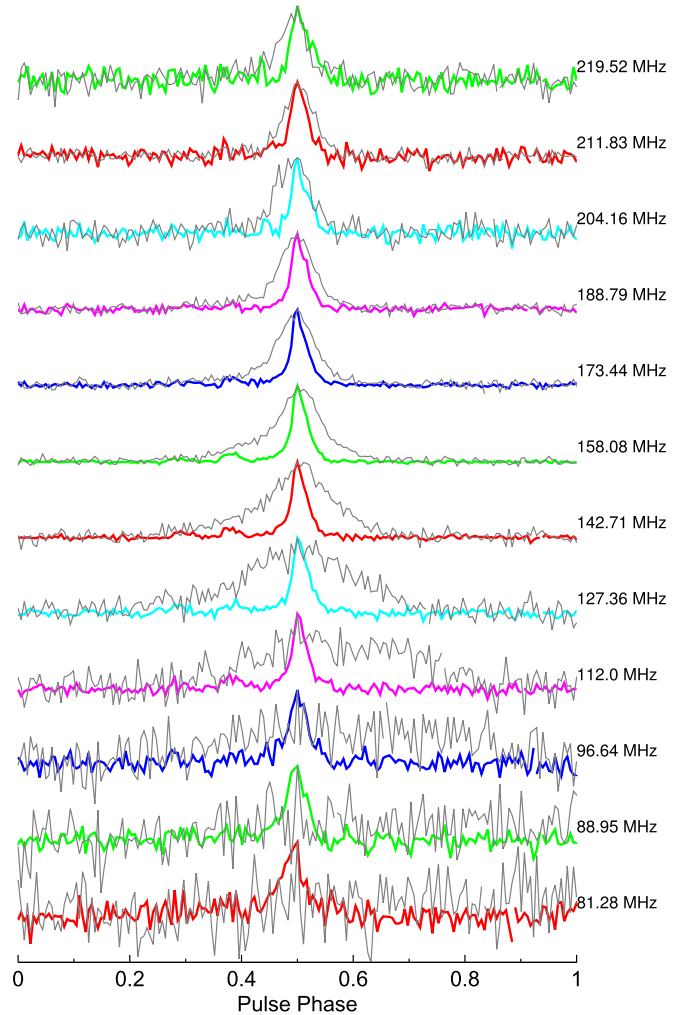


Figure 1. MWA detections of PSR J2241–5236 from observations made at MJD 57979. Data were coherently dedispersed at each of the 12×2.56 MHz bands. The pulsar is detected throughout the 80–220 MHz range; the resultant profiles (in color) are overlaid with the detections using the previous system, at 10 kHz resolution (in gray), where the pulse profile is significantly broadened due to residual dispersive smearing within 10 kHz channels (4% to $\sim 80\%$ of the pulse period).

5. Results and Discussion

PSR J2241–5236 has so far been primarily studied at frequencies above 700 MHz, with the Parkes telescope (Keith et al. 2011; Dai et al. 2015). Aside from a low S/N detection that was reported by Xue et al. (2017), there are no other low-frequency observations of this pulsar in the published literature. Unlike other bright southern MSPs such as PSRs J0437–4715 and J2145–0750 (e.g., Bhat et al. 2018), PSR J2241–5236 has a narrow pulse profile and shows little profile evolution within the MWA’s band. Figure 3 presents the frequency-averaged profile centered at 150 MHz, and we measure a 10% pulse width (W_{10}) of $\sim 150 \mu\text{s}$ at 158 MHz, which is comparable to $\sim 130 \mu\text{s}$ measured at Parkes frequencies (~ 1 –3 GHz).

In general, MSPs tend to show quite complex and rapid profile evolution with frequency (e.g., Dai et al. 2015; Bhat et al. 2018). In the case of J2241–5236, while the main pulse shows little evolution with frequency, MWA observations reveal an interesting dual-precursor type feature, which is less prominent at Parkes frequencies (see Figure 3). On a closer examination of Figures 1 and 2, it is evident that the precursor

¹¹ The measured 10% pulse widths $\sim 150 \mu\text{s}$ across our 80–220 MHz range.

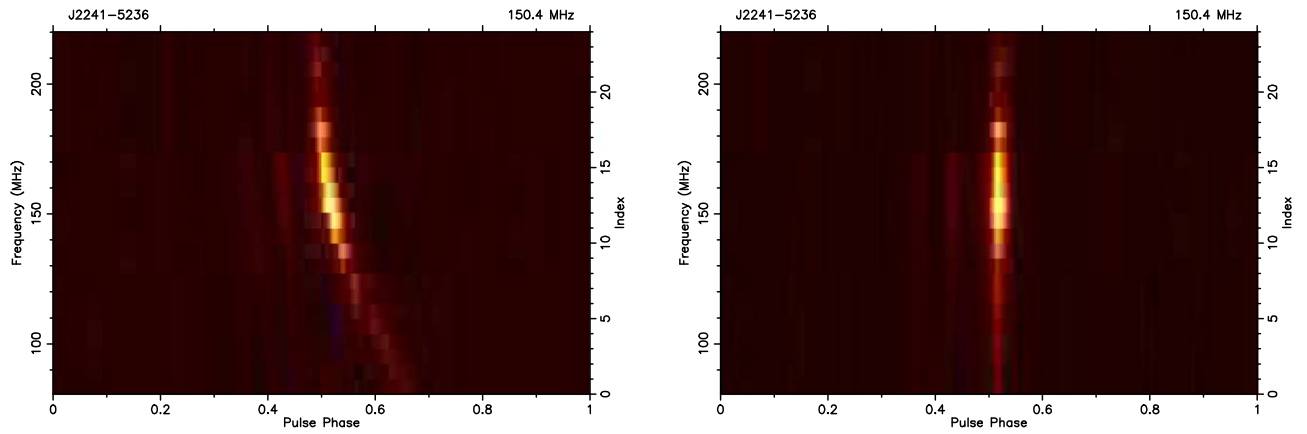


Figure 2. Detection of PSR J2241–5236 across the 80–220 MHz frequency range of the MWA from observations made at MJD = 57979. Plots showing pulse intensity as a function of frequency vs. pulse phase, where 12 sub-bands, each 2.56 MHz wide, at separations ~ 8 –16 MHz, are joined together. Left: data processed with the catalog DM of $11.41085 \text{ pc cm}^{-3}$ and the quadratic sweep of 0.4 ms implies an excess DM of $0.000667 \text{ pc cm}^{-3}$. Right: data reprocessed with the refined DM of $11.41151 \text{ pc cm}^{-3}$, demonstrating the MWA’s sensitivity to subtle DM variations.

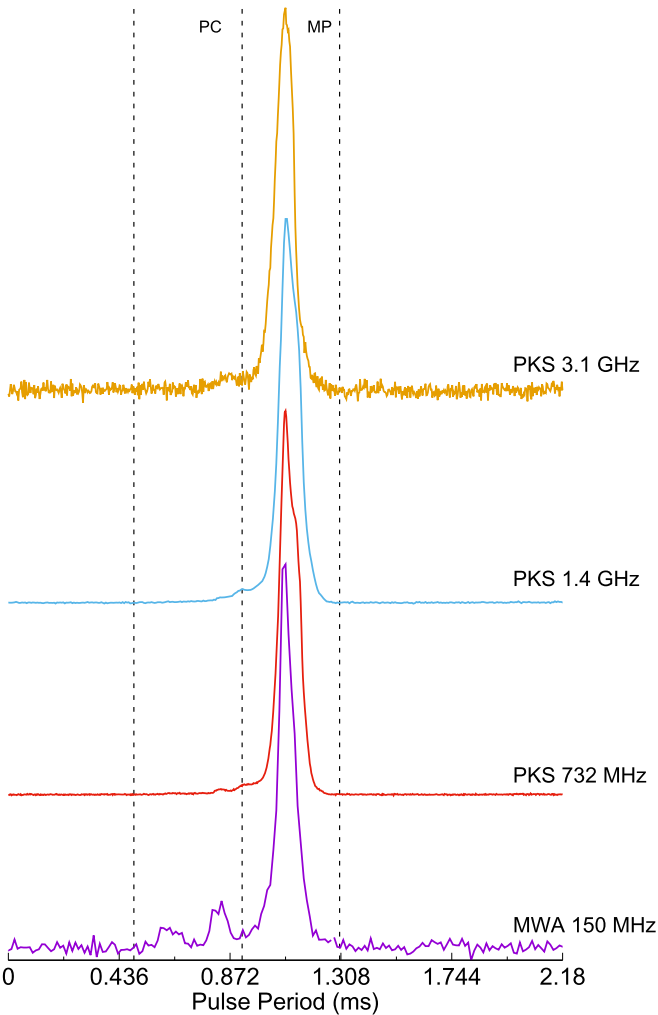


Figure 3. Integrated pulse profiles of PSR J2241–5236 at frequencies from 150 MHz to 3.1 GHz. The MWA profile has a time resolution of $\sim 8.5 \mu\text{s}$, whereas Parkes profiles (from Dai et al. 2015) have a time resolution of $\sim 2 \mu\text{s}$.

emission is persistent over a large fraction of the observed MWA band, where it is nominally seen at 10%–15% of the pulse peak. However, its relative phase appears to be slightly offset (leftward) compared to that seen at Parkes frequencies.

Table 2
DM Measurements from Three Observed Epochs

Date of Obs MJD	DM (pc cm^{-3})	$\sigma_{\text{DM}}^{\text{a}}$ (pc cm^{-3})	Post-fit Residual (μs)
57288	11.41165(3)	$(3-9) \times 10^{-5}$	12.6
57707	11.41162(6)	$(6-9) \times 10^{-6}$	1.4
57979	11.41151(2)	$(2-7) \times 10^{-6}$	0.8

Note. The catalog DM value for PSR J2241–5236 is $11.41085 \text{ pc cm}^{-3}$, with uncertainties of $3 \times 10^{-5} \text{ pc cm}^{-3}$.

^a The achievable DM precision (σ_{DM}) varies depending on the frequency lever arm, which ranges from ~ 140 to ~ 10 MHz in our analysis (see Table 1 and Figure 1).

This could possibly be due to the spectral evolution of the profile. Observations at intermediate frequencies (~ 300 –700 MHz) would be useful to further investigate this.

5.1. DM Measurements and Precision

We initially dedispersed the data using the catalog DM of $11.41085 \text{ pc cm}^{-3}$. This revealed a clear quadratic sweep of approximately 0.4 ms as seen in Figure 2. We subsequently reprocessed the data using our refined DM measurements, as summarized in Table 2. Our measured DMs are consistently larger than the catalog value. The average DM from all three observations is $11.411505 \text{ pc cm}^{-3}$, which may suggest an “excess” DM of $0.000655 \text{ pc cm}^{-3}$, compared to the catalog value as reported in Keith et al. (2011).¹²

Such subtle changes can in principle arise due to effects such as chromatic (frequency-dependent) DMs, as recently theorized by Cordes et al. (2016). The chromatic DM being a consequence of multipath scattering, in general, one may expect a dependence on the degree of scattering. However, our current observations (where we distribute the recording bandwidth to sample multiple spot frequencies across a large frequency range) are not ideal for a meaningful scintillation analysis. In any case, there has been some observational evidence in support of excess DM at low frequencies, e.g., in the case of PSR J2145–0750, for which MWA and LWA

¹² Based on timing data (~ 1 –2 GHz) taken over an ~ 15 month time span in 2009–2010.

measurements by Bhat et al. (2018) and Dowell et al. (2013) report a δDM of $0.006 \pm 0.003 \text{ pc cm}^{-3}$. More recently, DM variations have been reported for PSR J2219+4754 by Donner et al. (2019) and Lam et al. (2019) from LOFAR observations, and have been attributed to chromatic DMs, although their interpretations differ. With only limited observational efforts to date to investigate this important effect, routine observations with low-frequency instruments such as the MWA and LWA will be especially useful.

PSR J2241–5236 is a high-priority target for PTA applications (i.e., along the class of pulsars like J1909–3744 and J1744–1134). However, to date, there are no published measurements of temporal DM variations (on timescales of \sim months to years) for this pulsar. As can be seen from Table 2, our observations suggest DM variations, $\delta\text{DM} \sim 10^{-4} \text{ pc cm}^{-3}$, on timescales of ~ 1 –2 yr. Since the observed DM variation is subtle, multiple different sources of origin can be considered. For example, the solar wind is known to produce DM variations up to $\sim 10^{-5} \text{ pc cm}^{-3}$ (e.g., Kumar et al. 2013; Lam et al. 2016), when observations are made very close to the Sun. However, this seems unlikely, as our observations were made at large solar elongations ($\gtrsim 80^\circ$), and as such the pulsar is far from the ecliptic plane. There has been some recent evidence that the companion winds can modulate the DM for binary pulsars. PSR J2241–5236 is in a 3.5 hr, almost circular orbit with a low-mass ($\sim 0.01 M_\odot$) black widow type companion. We may therefore expect subtle variations in DM as a function of the orbital phase, especially in light of the recent work by An et al. (2018), who report orbital modulation in gamma-ray due to intra-binary shock emission. There has been observational evidence for such a black-widow-like system with an ablating companion producing DM variations, e.g., PSR B1957+20 (Fruchter et al. 1990). However, in the case of J2241–5236, no eclipses have been seen as the inclination angle is likely large (Keith et al. 2011), making this less probable. Moreover, due to our limited data and a sparse coverage of the orbit we refrain from making definitive comments on this.

The DM precision depends on the frequency lever arm, with the best precision achieved for the longest, which, in our case, is 80–220 MHz. As can be seen in Table 2, this is in the range $(2\text{--}6) \times 10^{-6} \text{ pc cm}^{-3}$, depending on the quality of detection. This is already an order of magnitude better than what is currently achievable at timing frequencies ($3 \times 10^{-5} \text{ pc cm}^{-3}$; Jones et al. 2017), and even the most recent work of Donner et al. (2019), who reach a similar level of precision. Since our analysis relied on the use of a single template (and not frequency-dependent templates that are ideal for wide-band timing), there is indeed scope for considerable improvement as we accrue more data with the MWA. Furthermore, the measured DM variation (δDM), is about ~ 3 –10 times larger than our measurement uncertainties (see Table 2), highlighting the MWA’s high sensitivity to measuring such subtle changes in DMs.

5.2. Spectral Behavior at Low Frequencies

The pulsar spectra generally follow a single power law $S_\nu \propto \nu^\alpha$, where S_ν is the flux density at the observing frequency ν and α is the spectral index. However, there are exceptions, where the spectral form tends to either steepen or flatten, or even turn over (e.g., Kramer et al. 1998; Maron et al. 2000; Jankowski et al. 2018). MSP spectra were initially reported to be steeper, compared to those of long-period pulsars (Toscano et al. 1998). However, the later work by Kuzmin & Losovsky (2001) claimed

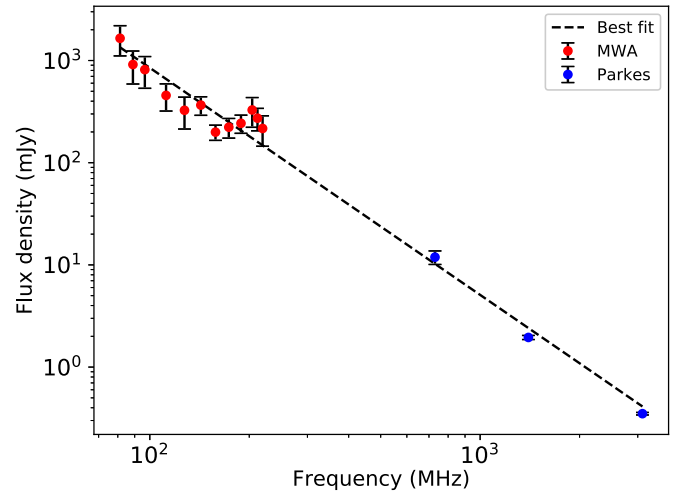


Figure 4. Flux density measurements of PSR J2241–5236 from 80 MHz to 3 GHz. For the MWA range (80–220 MHz), measurements are averaged over all three observations. The best-fit spectral index is $\alpha_{\text{MP}} = -2.25 \pm 0.10$, compared to $\alpha_1 = -2.12 \pm 0.04$ from Parkes measurements.

a lack of low-frequency spectral turnover for MSPs. More recent work by Dai et al. (2015) suggests a possible turnover for at least a few pulsars, and the work by Kondratiev et al. (2016), at frequencies below 300 MHz, suggests that for many MSPs their measured flux densities are lower than the predicted ones, again hinting at a possible spectral turnover.

Using the procedure explained in Section 4.2 we estimated the flux densities from our integrated pulse profiles. By combining the Parkes and MWA data, we estimated a spectral index for the main pulse (MP) $\alpha_{\text{MP}} = -2.25 \pm 0.10$. Since the precursor components (PC) are not prominent in the Parkes band, they were excluded from our analysis. Figure 4 presents the mean flux densities measured from multiple MWA observations (see Table 2) along with Parkes data from Dai et al. (2015). Parkes measurements are from a regularly sampled, six-year data set, whereas MWA measurements are from just three observations over a ~ 3 yr time span. Variability in measured flux densities between different observations at the MWA’s frequencies is generally within a factor of two, across the entire frequency range, and this is consistent with expectations from refractive scintillation at these low frequencies.¹³ The timescale for refractive interstellar scintillation (RISS), $\tau_{\text{riss}} = (\nu/\nu_{\text{diss}})\tau_{\text{diss}}$, where ν_{diss} and τ_{diss} are the frequency and timescale for diffractive interstellar scintillation, respectively (Rickett 1990). For our observations at 158 MHz (MJD = 57979), preliminary estimates are ~ 200 kHz for decorrelation bandwidth (ν_{diss}) and ~ 1000 s for timescale (τ_{diss}). Thus, we estimate a refractive timescale, $\tau_{\text{riss}} \sim 9$ days. The small number of observations and a sparse sampling of refractive scintillation cycles can therefore somewhat bias our flux density measurements, and this is reflected by the scatter in Figure 4. Nonetheless, since our observations were made in a distributed sub-band setup (i.e., 12×2.56 MHz spread over the 80–220 MHz range), our measurements at any given epoch are essentially independent (i.e., 3×12 independent measurements that constrain the low-frequency part of the spectrum in Figure 4). The combination of multiple independent

¹³ The modulations due to diffractive scintillation is $\sim 30\%$, based on our estimated scintillation parameters.

measurements, and multiple observations with a time separation much longer than the RISS timescale, effectively works to decrease any possible bias. Indeed, more observational data will help further refine these measurements and thus yield more robust estimates of the spectrum.

Our measured spectral index is consistent with one of the two estimates ($\alpha_1 = -2.12 \pm 0.04$) from Dai et al. (2015), which is the best fit to their observations made at three Parkes bands. Dai et al. (2015) also quote a much larger value for the spectral index, $\alpha_2 = -2.93 \pm 0.07$, when suitable weights are applied to longer observations. Incidentally, all these estimates are discrepant with the estimate from Murphy et al. (2017), who report $\alpha = -1.3 \pm 0.1$. This discrepancy is likely due to their use of comparatively less reliable measurements (at ~ 1 GHz) and the measurements from continuum imaging data (at lower frequencies).

A closer examination of Parkes data suggests that the spectrum is steeper for most of the main pulse ($-3.0 < \alpha < -2.5$), and shallower toward the trailing side of the main pulse (> -2.5 ; see Figure A24, Dai et al. 2015). Given the prominence of precursor emission ($\sim 10\%$ – 15% of the pulse peak, which corresponds to ~ 380 mJy at 158 MHz) in the MWA band, we can place an upper limit on its spectral index ($\alpha_{\text{PC}} < -3.7$), which may indicate a likely spectral steepening at low frequencies. The other plausible cause is possible frequency evolution of the pulse profile, which would require further detailed investigations using the wide-band instrumentation now available at the Parkes and Giant Metrewave Radio Telescopes, preferably from observations conducted simultaneously with the MWA.

The recent discoveries of MSPs at low frequencies (Bassa et al. 2017; Lynch et al. 2018) reaffirms the general trend of MSPs exhibiting steeper spectra, which is also consistent with our recent work (e.g., Bhat et al. 2018). This is encouraging from the perspective of finding new pulsars using current and next-generation low-frequency telescopes such as the low-frequency SKA.

6. Conclusions

The development of a new software beamformer for MWA pulsar processing has enabled high-quality low-frequency detections of the short-period MSP J2241–5236, a top-priority target for PTA applications. By inverting the PFB operation that was performed prior to the VCS recording, the new beamformer produces high-time resolution ($\sim 1 \mu\text{s}$) voltage time series data that are amenable for phase-coherent dedispersion. With the resultant high-fidelity detections, we are able to achieve a timing precision of the order $\sim 1 \mu\text{s}$ at the low frequencies of the MWA, which allowed us to measure the pulsar DM with a very high precision, of the order of $(2\text{--}6) \times 10^{-6} \text{ pc cm}^{-3}$. This provides an excellent demonstration of the MWA’s capability to monitor subtle DM variations ($\sim 10^{-4} \text{ pc cm}^{-3}$) reliably for southern pulsars. The DM precision, and the sensitivity to DM changes, can be further improved in the future as more observations accrue and the use of frequency-dependent templates becomes possible. Given that PSR J2241–5236 is quickly emerging as one of the high-priority targets for current and future PTAs, DM excess and/or variation at the level of $\sim 10^{-4} \text{ pc cm}^{-3}$ deserves particular importance, as any residual uncorrected DM variations can impact the achievable timing precision.

Our observations also reveal a dual-precursor type feature in the pulse profile, which appears to be far less prominent at higher frequencies from Parkes. The precursor emission



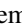






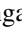

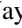
appears to have a steeper spectrum than that of the main pulse. The estimated spectral index for the pulsar’s main pulse emission $\alpha_{\text{MP}} = -2.25 \pm 0.10$, and there is no sign of any turnover within the observed MWA band. This is consistent with the general trend from other recent studies of MSPs and is promising for their low-frequency studies in general, particularly for finding new ones at low frequencies.

We would like to thank an anonymous referee for valuable comments and suggestions that helped to improve the clarity and presentation of this paper. This scientific work makes use of the Murchison Radio-astronomy Observatory, operated by CSIRO. We acknowledge the Wajarri Yamatji people as the traditional owners of the Observatory site. Support for the operation of the MWA is provided by the Australian Government (NCRIS), under a contract to Curtin University administered by Astronomy Australia Limited. We acknowledge the Pawsey Supercomputing Centre, which is supported by the Western Australian and Australian Governments. Parts of this research were conducted by the Australian Research Council Centre of Excellence for All-sky Astrophysics (CAASTRO), through project no. CE110001020. D.K. acknowledges support from the Curtin International Postgraduate Research Scheme. R.M.S. acknowledges support through ARC grant CE170100004. D.L.K. was supported by the NANOGrav project, which receives support from NSF Physics Frontier Center award number 1430284.

Facility: The MWA and Parkes radio telescope facilities.

Software: This work made use of the following software packages: DSPSR (van Straten & Bailes 2011) and PSRCHIVE (Hotan et al. 2004; van Straten et al. 2012).

ORCID iDs

D. Kaur  <https://orcid.org/0000-0003-4879-1019>
 N. D. R. Bhat  <https://orcid.org/0000-0002-8383-5059>
 S. E. Tremblay  <https://orcid.org/0000-0001-7662-2576>
 R. M. Shannon  <https://orcid.org/0000-0002-7285-6348>
 S. J. McSweeney  <https://orcid.org/0000-0001-6114-7469>
 A. P. Beardsley  <https://orcid.org/0000-0001-9428-8233>
 M. Johnston-Hollitt  <https://orcid.org/0000-0003-2756-8301>
 D. L. Kaplan  <https://orcid.org/0000-0001-6295-2881>
 M. F. Morales  <https://orcid.org/0000-0001-7694-4030>
 S. J. Tingay  <https://orcid.org/0000-0002-8195-7562>
 C. M. Trott  <https://orcid.org/0000-0001-6324-1766>
 R. B. Wayth  <https://orcid.org/0000-0002-6995-4131>

References

- An, H., Romani, R. W., & Kerr, M. 2018, *ApJL*, 868, L8
 Bailes, M., Barr, E., Bhat, N. D. R., et al. 2018, arXiv:1803.07424
 Bassa, C. G., Pleunis, Z., Hessels, J. W. T., et al. 2017, *ApJL*, 846, L20
 Bhat, N. D. R., Cordes, J. M., Camilo, F., Nice, D. J., & Lorimer, D. R. 2004, *ApJ*, 605, 759
 Bhat, N. D. R., Ord, S. M., Tremblay, S. E., et al. 2014, *ApJL*, 791, L32
 Bhat, N. D. R., Ord, S. M., Tremblay, S. E., McSweeney, S. J., & Tingay, S. J. 2016, *ApJ*, 818, 86
 Bhat, N. D. R., Tremblay, S. E., Kirsten, F., et al. 2018, *ApJS*, 238, 1
 Cordes, J. M., & Shannon, R. M. 2010, arXiv:1010.3785
 Cordes, J. M., Shannon, R. M., & Stinebring, D. R. 2016, *ApJ*, 817, 16
 Crochiere, R. E., & Rabiner, L. R. 1983, *Multirate Digital Signal Processing* (Englewood Cliffs, NJ: Prentice-Hall)
 Dai, S., Hobbs, G., Manchester, R. N., et al. 2015, *MNRAS*, 449, 3223
 de Oliveira-Costa, A., Tegmark, M., Gaensler, B. M., et al. 2008, *MNRAS*, 388, 247

- Demorest, P. B., Ferdman, R. D., Gonzalez, M. E., et al. 2013, *ApJ*, 762, 94
- Donner, J. Y., Verbiest, J. P. W., Tiburzi, C., et al. 2019, *A&A*, 624, A22
- Dowell, J., Ray, P. S., Taylor, G. B., et al. 2013, *ApJL*, 775, L28
- Fruchter, A. S., Berman, G., Bower, G., et al. 1990, *ApJ*, 351, 642
- Hankins, T. H., & Rickett, B. J. 1975, *MComP*, 14, 55
- Hobbs, G., Edwards, R., & Manchester, R. 2006, *ChJAS*, 6, 189
- Hotan, A. W., van Straten, W., & Manchester, R. N. 2004, *PASA*, 21, 302
- Jankowski, F., van Straten, W., Keane, E. F., et al. 2018, *MNRAS*, 473, 4436
- Janssen, G., Hobbs, G., McLaughlin, M., et al. 2015, in *Advancing Astrophysics with the Square Kilometre Array (AASKA14) (Trieste: SISSA)*, 37
- Jones, M. L., McLaughlin, M. A., Lam, M. T., et al. 2017, *ApJ*, 841, 125
- Keith, M. J., Johnston, S., Ray, P. S., et al. 2011, *MNRAS*, 414, 1292
- Kirsten, F., Bhat, N. D. R., Meyers, B. W., et al. 2019, *ApJ*, 874, 179
- Kondratiev, V. I., Verbiest, J. P. W., Hessels, J. W. T., et al. 2016, *A&A*, 585, A128
- Kramer, M., Xilouris, K. M., Lorimer, D. R., et al. 1998, *ApJ*, 501, 270
- Kumar, U., Gupta, Y., van Straten, W., et al. 2013, in *IAU Symp. 291, Neutron Stars and Pulsars: Challenges and Opportunities after 80 years*, ed. J. van Leeuwen (Cambridge: Cambridge Univ. Press), 432
- Kuzmin, A. D., & Losovsky, B. Y. 2001, *A&A*, 368, 230
- Lam, M. T., Cordes, J. M., Chatterjee, S., et al. 2016, *ApJ*, 821, 66
- Lam, M. T., Lazio, T. J. W., Dolch, T., et al. 2019, arXiv:1903.00426
- Lam, M. T., McLaughlin, M. A., Cordes, J. M., Chatterjee, S., & Lazio, T. J. W. 2018, *ApJ*, 861, 12
- Levin, L., McLaughlin, M. A., Jones, G., et al. 2016, *ApJ*, 818, 166
- Lorimer, D. R., & Kramer, M. 2004, *Handbook of Pulsar Astronomy* (Cambridge: Cambridge Univ. Press)
- Lynch, R. S., Swiggum, J. K., Kondratiev, V. I., et al. 2018, *ApJ*, 859, 93
- Manchester, R. N., Hobbs, G., Bailes, M., et al. 2013, *PASA*, 30, e017
- Maron, O., Kijak, J., Kramer, M., & Wielebinski, R. 2000, *A&AS*, 147, 195
- McSweeney, S. J., Bhat, N. D. R., Tremblay, S. E., Deshpande, A. A., & Ord, S. M. 2017, *ApJ*, 836, 224
- Meyers, B. W., Tremblay, S. E., Bhat, N. D. R., et al. 2017, *ApJ*, 851, 20
- Mitchell, D. A., Greenhill, L. J., Wayth, R. B., et al. 2008, *ISTSP*, 2, 707
- Murphy, T., Kaplan, D. L., Bell, M. E., et al. 2017, *PASA*, 34, e020
- Oppenheim, A. V., Schafer, R. W., & Buck, J. R. 1999, *Discrete-time Signal Processing* (2nd ed.; Upper Saddle River, NJ: Prentice-Hall)
- Ord, S. M., Tremblay, S. E., McSweeney, S. J., et al. 2019, *PASA*, 36, e030
- Pennucci, T. T. 2019, *ApJ*, 871, 34
- Rickett, B. J. 1990, *ARA&A*, 28, 561
- Shannon, R. M., & Cordes, J. M. 2017, *MNRAS*, 464, 2075
- Taylor, G. B., Ellingson, S. W., Kassim, N. E., et al. 2012, *JAI*, 1, 1250004
- Tingay, S. J., Goetze, R., Bowman, J. D., et al. 2013, *PASA*, 30, e007
- Toscano, M., Bailes, M., Manchester, R. N., & Sandhu, J. S. 1998, *ApJ*, 506, 863
- Tremblay, S. E., Ord, S. M., Bhat, N. D. R., et al. 2015, *PASA*, 32, e005
- van Haarlem, M. P., Wise, M. W., Gunst, A. W., et al. 2013, *A&A*, 556, A2
- van Haasteren, R., Levin, Y., Janssen, G. H., et al. 2011, *MNRAS*, 414, 3117
- van Straten, W., & Bailes, M. 2011, *PASA*, 28, 1
- van Straten, W., Demorest, P., & Osłowski, S. 2012, *AR&T*, 9, 237
- Wayth, R. B., Tingay, S. J., Trott, C. M., et al. 2018, *PASA*, 35, e033
- Xue, M., Bhat, N. D. R., Tremblay, S. E., et al. 2017, *PASA*, 34, e070